An effective probabilistic simulation of the turbulent flow and combustion in axisymmetric furnaces

AN EFFECTIVE PROBABILISTIC SIMULATION OF THE TURBULENT FLOW AND COMBUSTION IN AXISYMMETRIC FURNACES

Th.T.A. Paauw, A.J. Stroo, C.W.J. van Koppen
Laboratory for Thermal Power Engineering
Delft University of Technology
Rotterdamseweg 139A
Delft, The Netherlands

ABSTRACT

The conservation equations governing the flow field and the combustion process in isothermal and in diffusion controlled combusting confined flows are solved using a numerical finite difference technique; the results are compared with measurements.

The combustion process of the hydrocarbon fuel has been modelled by using instant reaction with fluctuations in the mixture fracture, and with three different assumptions for the chemical conditions: frozen chemistry, equilibrium chemistry and partial equilibrium chemistry.

Attention is paid to the formation of nitrogen oxides, and it is shown that in hydrocarbon diffusion flames a substantial amount of the NO formed is due to 'prompt NO' formation. For this process an effective model is presented.

1. INTRODUCTION

During the last decade considerable effort has been devoted to the modelling of furnace phenomena. In general two distinct lines of approaching the problem can be observed.
Some authors have tried to model the furnace by dividing it into several separate sections, each representing a simple system, s.a. well stirred or a plug flow reactor [1]. Although such methods are useful for the prediction of the trends in furnace behaviour or pollutants formation, additional model assumptions and empirical data are often required for particular calculations.
On the other hand methods have been developed that simulate the furnace performance in more detail, generally by solving the conservation equations in finite difference form [2-4]. These methods lead to a fair prediction of the influence of furnace geometry and configuration dependent phenomena s.a. furnace heat transfer and flame furnace wall interaction. However, these more sophisticated models also require some assumptions, normally regarding the turbulence model, the radiation model and the combustion model.
In the present work such a detailed method is used for the prediction of the completely diffusion controlled combustion of gaseous hydrocarbons in an axisymmetrical combustion chamber. Several combustion models are investigated, all based on instant reaction combined with scalar fluctuations. The main scalar being in this case the socalled mixture fraction, and particularly, attention is paid to the accurate prediction of the fluctuations of this scalar.
In this framework the mixing process of a scalar and the production of scalar fluctuations in an isothermal combustor geometry is firstly investigated by comparing the results of numerical calculations with extensive measurements by BECKER [5-6].
Furthermore, the assumptions concerning the combustion process are investigated in a detailed comparison between experimental and numerical data for natural gas flames.
Finally, the developed models are tested by comparison of calculations with measurements obtained in the Delft furnace for a low NO_x burner geometry.

2. MATHEMATICAL AND PHYSICAL ANALYSIS

2.1. Basic equations.

The calculation procedure consists of solving the partial differential equations representing the conservation of the time averaged flow properties in an axisymmetrical flow geometry. The general, elliptic form of these equations can be expressed as:

$$\frac{\partial}{\partial x}(\rho_\phi u\phi) + \frac{1}{r}\frac{\partial}{\partial r}(\rho_\phi v r\phi) = \frac{\partial}{\partial x}(\mu_\phi \frac{\partial \phi}{\partial x}) + \frac{1}{r}\frac{\partial}{\partial r}(\mu_\phi r \frac{\partial}{\partial r}\phi) + S_\phi \qquad (1)$$

in which u and v represent axial and radial velocity, and ϕ a flow property, with μ_ϕ as its viscosity and S_ϕ as its sourceterm.

In the case of furnace calculations ϕ represent subsequently (u, v) axial and radial velocity, (k, ε) the turbulent kinetic energy and its dissipation, h, the stagnation enthalpy, (R_x^k, R_r^k) the radiant heat flux in the x and r direction for radiant gas k, ($\bar{Y}_f$, $\bar{Y}_f'^2$) the mixture fraction and its root mean square value and finally Y_{NO}, the mass fraction of thermal NO.

The values of ρ_ϕ, μ_ϕ and S_ϕ are given in table I. Constants necessary to solve these equations are given in table II.
When no recirculation takes place, as in the case of free diffusion flames, the second form on the right-hand side of (1) can be omitted, transforming the partial differential equation to a parabolic form, which is easier to solve numerically.
For the solution of equation (1) it is necessary to define boundary conditions; at the axis of symmetry (r = 0) these are: v = 0 and $\partial\phi/\partial r = 0$ for all other quantities, at the solid boundary empirical wall functions can be used to relate $(\partial\phi/\partial r)$ to the local values of ϕ, for u, v, k, ε and h [2, 7], and for R_x^k, R_r^k [8]; the other values of ϕ are set to zero. At the exit of the duct and furnace calculations $(\partial\phi/\partial r)$ was assumed to be zero, and at the entrance all variables ϕ were specified.

2.2. Turbulence model.

The two-equation turbulence model used in the present work is based on the solution of the equations for the turbulent kinetic energy k and its dissipation rate ε; in this model the logic assumption for the turbulent viscosity is: $\mu_e = C_D \rho k^2/\varepsilon$. This viscosity has to be added to the laminar viscosity.
The chosen model had been shown to give good predictions in boundary layer type flows [9], and also in more strongly elliptic flows of the same geometry as has been used here [2, 10].
Because of the uncertainties in the combustion model more refined turbulence models are judged to be over-sophisticated at this stage of the development.

2.3. Radiation model.

The four-flux radiation model adapted here is based on the formulation of GOSMAN e.a. [8], which reduces the original four equations for the radiation fluxes in four directions, $I^k_{x\pm}$ and $I^k_{r\pm}$ for radiant gas k, to two equations governing the distribution of the sum parameters $R^k_x = (I^k_{x+} + I^k_{x-})/2$, and $R^k_r = (I^k_{r+} + I^k_{r-})/2$. Although this formulation is efficient a deficiency can be the uncoupling of the fluxes in radial and axial direction.
Nevertheless summations of radial and axial fluxes, representing fluxes in directions under 45^0 with the symmetry axis, are evidently coupled. Also the dependency of $\mu_{R^k_r}$ on r correctly represents the consequences in radial direction of an anisotropic flux distribution.
Moreover the physical constants to be applied to the scattering and absorption of the calculus are uncertain, not at least because of the occurrence of luminous radiation.
Therefore scattering has to be assumed negligible, and two models for the absorption and emission coefficients have been tested. In a first model the absorption and emission constant have simply been chosen constant ($\alpha_1 = \varepsilon_1 = 4$), representing a one gray radiating gas. In a second model the constants have been assumed to be temperature and mixture dependent (α_k (Y_{CO_2}, Y_{H_2O}, ρ, T) and ε_k (Y_{CO_2}, Y_{H_2O}, ρ, T) for gas k) in a one clear, three gray gas formulation for natural gas developed and used by the IFRF [11] for natural (Groningen) gas in similar calculations.

2.4. Combustion models.

In the literature concerning combustion models two categories of models have been proposed. The first category consists of models in which the governing parameter is the fuel mass fraction. The conservation equation for the fuel mass fraction is solved using an effective source term, being either an Arrhenius type reaction rate or a flow pattern dependent reaction rate, s.a. the eddy break-up rate proposed by SPALDING [2] or in a different way by BRAY [12]. These models seem to be particularly suited for modelling premixed flames because there the effective reaction rate is the controlling factor.
In diffusion flames, however, the mixing process is much slower then the chemical reaction. Consequently the combustion process is controlled by mixing, the reaction rate can be assumed as infinitely fast, and a parameter like the mixture fraction, defining the mixing process, controls the reaction.
The relation between the reaction process and the mixture fraction in this case can be found via the quantity:

$$f = r.Y_{fu} - Y_{ox} \qquad (2)$$

where Y_{fu} and Y_{ox} denote fuel and oxidant mass fractions and r is the stoïchiometric mass ratio between fuel and oxidant.
The conservation equation governing the distribution of f has a source term equal to zero. Furthermore the following identity can be deduced:

$$Y_f = \frac{f - f_{ox}}{f_{fu} - f_{ox}} \qquad (3)$$

where Y_f in the fuel phase is equal to one, and in the oxidant phase equal to zero.
At the stoïchiometric conditions: $f_{st} = 0$, and $Y_{f_{st}} = 1/(r+1)$. For the Groningen natural gas used in our experiments r = 13.07 and $Y_{f_{st}} = .071$.
So far we have made no proposals for the reaction process, beside the fact that it is slower than the mixing process. In the paper three models will be discussed: the well known frozen composition model [2], the equilibrium composition model and a so-called partial equilibrium composition model.

2.4.1. Frozen composition model (model 1).

In this model it is assumed that the infinitely fast reaction is restricted to an infinitely small reaction zone, situated at the surface where $Y_f = Y_{f_{st}}$. Outside this reaction zone the reaction is considered to be completely quenched, and the composition is in effect frozen.
Under these assumptions it is a simple matter to define mass fractions and temperatures, for example:

$$Y_{fu} = 0 \quad \text{for} \quad Y_f < Y_{f_{st}}$$

and

$$Y_{ox} = 0 \quad \text{for} \quad Y_f > Y_{f_{st}} \tag{4}$$

The respective Y_{ox} and Y_{fu} can be found by means of equations (2) and (3). The temperature is calculated with help of the calculated enthalpy and an average value of the specific heat. The density follows from the equation for a perfect gas. Curves for the temperature and the oxygen concentration under adiabatic conditions are depicted in figure 1.

2.4.2. Equilibrium composition model (model 2).

In this model it is assumed that the infinitely fast reaction is not restricted to only a reaction surface, but does occur in the whole field, both for forward and backward reactions. This results in a local equilibrium composition, governed by the local equivalence ratio related to the mixture fraction and the local enthalpy. In this case it is not possible to obtain a straight forward relation between the relevant properties (e.g. the temperature) and the mixture fraction and enthalpy. To avoid this difficulty the following procedure has been adopted [14]. A two-dimensional mapping has been made of all relevant thermodynamic and chemical properties: temperature T, density ρ, viscosity μ, and mass fractions Y_{O_2}, Y_{CH_4}, Y_{CO_2}, Y_{CO}, Y_{H_2O}, Y_{H_2}, Y_{N_2}, and Y_O.

Using a least square method, this mapping has been fitted in Chebyshev double polynomials:

$$Y_i\,(h, Y_f) = \sum_{i=1}^{I} \sum_{j=1}^{J} a_{ij}\, T_i\,(h^*)\, T_j\,(Y_f^*) \tag{5}$$

in which h^* and Y_f^* denote normalised values of h and Y_f, whereas T_i denotes a Chebyshev polinomial of degree i and I and J have values up to eight.

Equation (5) represents an efficient instrument for the calculation of the equilibrium conditions, when the recurrence relations for Chebyshev polynomials are used. However, in the iterative procedure to solve the finite difference form of the partial differential equations, mentioned before, a much more economical prodecure is employed by making use of the mentioned two-dimensional mapping employing bilinear interpolation. Also in this case calculated curves of T and Y_{O_2} are given in figure 1 for adiabatic conditions.

It should be noted that the temperature sharply decreases at the rich side of the stoïchiometric point; the decrease coïncides with an increase in Y_{H_2} and Y_{CO}.

2.4.3. Partial equilibrium composition model (model 3).

In figure 1 experimental data obtained from mass fraction profiles, measured in attached turbulent natural gas diffusion flames [14] are also reported. From these results it appears that the equilibrium composition assumption gives temperatures that are too low, while the frozen composition temperatures are much too high. More surprising, however, are the molecular oxygen curves. Theoretically the O_2 mass fraction at fuel rich condition ($Y_f > 0.071$) should be essentially zero both in the frozen and the equilibrium condition and even taking into account the unmixedness the highest value for Y_{O_2} to be expected below near stoïchiometric conditions ($Y_f = .11$) is 1.5%, whereas values beyond 5% are measured.

Obviously nearly all fuel (mainly CH_4) is consumed, but due to the short residence time in the flame front only part of the O_2 has reacted, resulting in high CO en H_2 mass fractions.

Behind the flame front the further reaction of O_2 is apparently suppressed and a frozen composition is found but with a finite O_2 mass fraction.

The reason for the quenching lies in the fact that in hydrocarbon flames O_2 mainly reacts with H radicals, and as shown by BULAU a.o. [18] the OH, H and O radicals effectively almost fully recombine for $\phi > 1.65$ ($Y_f > .088$).

To take these effects into account a partial equilibrium hypothesis is introduced, stating that oxygen in the fuel rich region does not react and so gives a constraint. The other species concentrations and the temperature have been calculated based on an equilibrium assumption with the constraint O_2 concentration. In figure 1b this hypothesis is illustrated by a straight line through the measured data points and gives a value at $Y_f = Y_{f_{st}}$ of $Y_{O_2} = 4\%$.

The calculated equilibrium temperature curve following from the quenched equilibrium hypothesis, using this Y_{O_2} constraint, is drawn in figure 1a and is seen to compare favourable with the measured data.

On behalf of further flame calculations the most relevant species and thermodynamic properties were calculated for quenched equilibrium conditions as function at the enthalpy and the mixture fraction, and also transformed in Chebychev polynomials in the way, explained in section 2.4.2.

2.5. Nitrogenoxide formation model.

In diffusion flames it is often assumed that most of the nitrogenoxide is found by high temperature reaction between oxygen and nitrogen molecules and atoms. This so-called thermal NO formation is usually based on the Zeldovich mechanism, with reaction rate:

$$\dot{w}_{NO}\,(Y_f) = 2k_z\,\rho\,\frac{Y_{N_2}(Y_f)}{M_N}\cdot\frac{Y_O\,(Y_f)}{M_O}\,\exp\,(-E_z/T(Y_f)) \tag{6}$$

with $k_z = 10.^{11.15}$ and $E_z = 37.5.10^3$, M_{N_2} and M_O denote the molecular weights.

The atomic oxygen mass fraction may be calculated either by the assumption of chemical equilibrium between molecular and atomic oxygen for the frozen chemistry models or by using equations like (5) for the equilibrium chemistry models.
In calculations for natural gas diffusion flames we found that especially for the equilibrium models the calculated thermal NO mass fraction was much smaller than the measured NO mass fraction. This may indicate that 'super equilibrium' oxygen concentration (see 2.4.3) play a role. Another possible explanation is 'prompt NO', often neglected in diffusion flames studies. As 'prompt NO' is formed only inside the reaction zone a frozen flow composition description for calculating the additional formation of thermal NO can be used. To test this last assumption measured NO mass fractions in attached natural gas diffusion flames are plotted against the mixture fraction in figure 2. This has been done for several values of both the Froude number ($Fr = u^2/gD$, with burner velocity u and burner diameter D, representing the influence of buoyancy forces on the flame and the Damhöhler number ($Da = (D/u)/\tau_c$, with τ_c as a critical combustion time, chozen here to be 5.10^{-5} s, the characteristic blow-out time of a homogeneous reactor), representing the influence of shear on the reaction process. From figure 2 it is clear that a correlation between Y_{NO} and Y_f does exist. The "too low" experimental NO values on the fuel richside can be explained by the fact that 'prompt NO' is partly preceeded by HCN [25], not measured here. The higher values of NO for fuellean mixture can be explained by the influence of additional thermal NO. The introgenoxide mass fraction at the stoïchiometric Y_f value (x_{NO} = 38 ppm) compares well with the 'prompt NO' concentrations measured in premixed stoïchiometric hydrocarbon flames [19]. The thin line in figure 2 drawn through the full circles represents a slightly lifted flame ($x_{ign}/D = 3.5$). It is clear that in this case the constrained, unreacted oxygen did not produce NO and the correlation mentioned above and drawn in figure 2 has to be changed, using the Y_f value of the ignition-point. In the following calculations both the thermal NO formation and the frozen flow 'prompt NO' contribution have been determined and added to give a total NO mass fraction.

2.6. Probability formulation of the mixing process.

The usefulness of a probability description of flames is illustrated by figure 1a where small fluctuations in Y_f around the stoïchiometric value result in large fluctuations in temperature, especially in the case of the equilibrium models. By reverse it is evident that momentary temperatures can be much higher than the average temperatures, resulting e.g. in instantaneous reaction rates that are orders of magnitude higher than those based on the average temperature.
Time average flow properties, the spatial distributions of which prescribed by equation (1), can be reaveraged as moments of the probability density function (PDF) governing the time dependent behaviour of the observed property. When a gaussian PDF is assumed the first and second moment of the PDF (representing the mean value and the root mean square value) completely determine the PDF. In our calculations such an assumption has been made for the PDF of the mixture fraction; the fact that Y_f can not be lower than the oxidant value or higher than the fuel value being taken into account by the use of a clipped gaussian shape, following LOCKWOOD e.a. [20]. From the PDF for the mixture fraction, $P(Y_f)$, the PDF for the temperature: P(T) can simply be derived by putting:

$$P(T)\,|dT| = P(Y_f)\,|dY_f| \tag{7}$$

The contributions to P(T) above and below the stoïchiometric value of Y_f have to be added. In figure 3 measurements of P(T) in natural gas diffusion flames [15], around the stoïchiometric reaction zone are shown and compared with the results of calculations. Each calculated curve is based on 16 points, (smoothed histograms, being composed of 16 bars) obtained by using calculated $\overline{Y_f}$ and $\overline{Y_f'^2}$ ($= Y_f'$) values and assuming a clipped gaussian PDF. Also here it is clear that the partial equilibrium flow, gives the better results by imposing a certain upper temperature limit (T ~ 1900 K) much lower than the adiabatic value (T = 2210 K).
Using equation (5) representing the combustion models and a Schwab-Zeldovich coupling function between h and Y_f [21]: $h = \beta(Y_f)$ and assuming that the Lewis number unity, the mean concentrations for the chemical properties can be defined by:

$$\overline{Y_i} = \int_0^1 Y_i\,(\beta(Y_f),\, Y_f)\; P(Y_f)\; dY_f \tag{8}$$

with i = O_2, N_2, CH_4, H_2O, H_2, CO, CO_2 and O. The same procedure is followed for the physical properties T, ρ and μ and for the 'prompt NO', where the linear relation drawn in figure 2 (thick line) has been applied to determine $Y_{NO}(Y_f)$.

The formation of thermal NO is governed by the averaged source term (6):

$$\overline{\dot{w}_{NO}} = \int_0^1 \dot{w}_{NO}\,(Y_f)\; P(Y_f)\; dY_f \tag{9}$$

source terms for the four flux models are formulated as:

$$\overline{\varepsilon_k T^4} = \int_0^1 \varepsilon_k\,(Y_f)\; T^4\,(Y_f)\; P(Y_f)\; dY_f \quad \text{and}$$

$$\overline{\alpha_k} = \int_o^1 \alpha_k (Y_f) P(Y_f) dY_f \qquad (10)$$

In (9) and (10) it is anticipated that the temperature, density and concentration dependencies can be expressed in a mixture fraction depencency.

2.7. Solution procedure.

To solve differential equations represented by equation (1) and table I, these equations are expressed in finite difference form and solved by the algorithms for the elliptic case and the parabolic case as given in respectively [22] and [23].
The calculations for the elliptic case were performed with a 20 x 20 nodes grid geometry. The number of iterations required to reach the convergion criterion defined in [22] was 300 in the case of isothermal confined flow. For the free jet diffusion flame with a simple model for the absorbtion and emission coefficients it reached 600 and for the case of more elaborate radiation constants, up to 1000. This same number of iterations was required for confined combustion calculations. The use of a combustion model led to an increase of necessary computing time per iteration with a factor of two compared with isothermal flow calculations. The elaborate radiation model led to an increase with a factor of three. The parabolic scheme for the free jet diffusion flames calculation was two orders of magnitude faster than the elliptic scheme however.

3. RESULTS AND COMPARISON WITH EXPERIMENTS

From the previous paragraphs concerning the combustion models and the introduction of the PDF it is clear that the mixture fraction and its fluctuations play an important role in the calculation procedure.
Mostly the stoichiometric value of the mixture fraction is small (natural gas: $Y_{f,st} = 0.071$) which means that small variations in the gradient slope of the axial Y_f profiles result in large variations in the predicted temperature curves. Confinement and recirculation strongly influence the accuracy of the prediction of the mixture fraction field and therefore the elliptic program was first tested for isothermal confined jets. Subsequently unconfined diffusion flames have been calculated with both the parabolic and the elliptic program in order to test the accuracy of the latter program and the influence of the grid arrangement, and for the comparison of the combustion models with experiments. At last comparison is made between furnace calculations and measurements.

3.1. Confined isothermal jet calculations.

To verify the equations that govern the mixture fraction and its fluctuations in a confirmed flow we decided first to compare calculations in isothermal flow with measurements. The only available experimental results in confined jet flow providing information about the mixture fraction and its fluctuations are those of BECKER [5], [6], [16].
The results also concern detailed measurements of the mean flow pattern and the static wall pressure. The data have been obtained in a cylindrical duct (.197 m diameter, 1.25 m length, smooth wall), in the center of which an air jet initial velocity $u_{c,o}$, (uniform profile, 6.35 mm diameter) was situated, surrounded by a secondary, uniform ground stream (velocity $u_{w,o}$).

The calculations have been carried out for different combinations of primary and secondary velocities, yielding Craya-Curtet numbers of 1.22, .673, .345 and .212. These numbers correspond to flow patterns with increasing recirculation. The Ct number is defined as:

$$Ct = \bar{u}_f / u^*_o \text{ , with } u^{*2}_o = \overline{u_f^2} - (u^2_{w,o} + \bar{u}^2_f)/2,$$

where $\bar{u}$ and $\overline{u^2}$ are the area-averaged velocities [5], and u^{*2}_o can be regarded as a measure of the non-uniformity of the momentum flux distribution at the inlet.
The ducted flow can be regarded as being devided into three regions: a region of jet growth, a recirculation zone, and post-jet mixing zone. This becomes particularly clear from the axial profiles of $u_o/(u-u_w)$ and $Y_{fo}/(Y_f-Y_{f,w})$ given in figure 4 and 6, where u_w and $Y_{f,w}$ refer to the ground stream.
The relation between the reciprocals of mixture fraction and velocity and the axial distance is lineair in the jet growth region, whereas the curves bend steeply upwards in the final region. Here the ground stream velocity tends to the velocity at the axis. Especially for lower Ct numbers there is a good agreement between calculated and measured data. The changes in mixing regime are also well represented in the static pressure profile (figure 5) where the position of the sudden increase in pressure corresponds with the eye of the recirculation zone. However, the absolute values of the pressure rise are conspiciously high in comparison to the measured results, indicating that overprediction of wall friction or internal friction in the recirculation zone does possible occur. It should be noted that the pressure rise does sensitively depend on the profile of the nozzle flow, here assumed to be essential uniform. Similar overpredictions of the pressure are also reported by KANG e.a. [10] using the same method in confined flows with comparable Ct numbers.
The post-jet mixing behaviour is mainly characterised by the mixture fraction fluctuations; some results are depicted in figure 7. Beyond the recirculation zone, i.e. when the jet has reached the wall, the production of fluctuations diminishes and dissipation results in their decrease.
This is reproduced in the calculations for the lower Ct numbers, allthough the maximum predicted fluctuation intensity at low axial distances are higher than those measured by BECKER [30]. Measurements in free jets by Haberda show a better agreement. For the lower Ct numbers investigated the maximum influence of the mixture fraction fluctuations on the temperature field can be expected to occur in the reaction zone around $Y_{f,st}$ considering the combustion model that was applied. For natural gas, $Y_{f,st} = .071$, corresponds with $x/D_f > 15$; in this region the predictions are fairly correct.

For the highest Ct number the axial profile of mixture fraction fluctuations is not influenced by the confinement and resembles the calculated profiles in free jets using the same set of partial differential equations as in table I but in a parabolic form [17], [24]. In the last case the value of $Y_f'/\bar{Y}_f$ on the axis is only slightly smaller than the value of .227 obtained here.

3.2. Free jet diffusion flames.

In order to validate the combustion models described before, we decided to compare calculations for the relatively simple turbulent diffusion flame with detailed measurements concerning the temperature, mass fractions, velocity and radiation field in such flames. For the comparison a vertical natural gas flame with $D = 10^{-2}$ m, $\bar{u}_o$ = 20 m/s, Re = 14500, Fr = 3900 and Da = 21 was selected; because of both the considerable shear stress and buoyancy in this flame no local laminarisation of the flame front is to be expected.

3.2.1. Influence of the numerical method.

The numerical predictions for the flame have been obtained in two ways: using a parabolic flow program and using a elliptical program, with respectively a 20 x 25 and a 21 x 30 grid arrangement. The axial and radial grid locations have been chosen finely distributed around the burner, both with a node density for grid II two times higher than for grid I.
Presumably in this region the grid II is smaller than the turbulent macrolentgh scale whereas it is slightly larger in grid I. The results indicate that an underprediction of the production of turbulence follows from the larger grid spacing. The outer radial grid point (the wall) is situated at a distance of .5 m from the burner. Here a secondary flow with a velocity of .2 m/s is assumed in combination with zero wall gradients. Varying these assumptions within reasonable limits did not influence the flame structure.
The mean axial temperatures calculated with combustion model 2 and the different numerical schemes are presented in figure 8. The coarse grid I obviously leads to a slower mixing process than the finer grid II, resulting in a stoichiometric mixture and a maximum temperature further downstream. Using grid II leads to an upstream shift of this point both for the elliptic and the parabolic scheme. By combining the parabolic and the elliptic scheme in an additional calculation it was shown that the influence of the grid spacing was mainly restricted to the region between the burner mouth and x/D = 5. Using the results of the fine grid parabolic scheme in this point as initial values for coarse grid elliptic scheme calculations further downstream brought the position of the maximum temperature within 10% from the position obtained with a completely fine grid calculation. The proceeding results show that for turbulent, diffusion flame-like combustion processes (free jet flow or confined flow with a large Ct number) a carefull choise has to be made for the grid location in high intensity mixing zones. Grid spacings as given for grid II have been used for all the following combustion calculations.

3.2.2. Influence of the combustion model.

With the fine grid spacing the diffusion flame defined before has been recalculated with the frozen composition and the partial equilibrium combustion model. The predicted temperature profiles, velocity and mixture profiles both using the parabolic and elliptic computation scheme are presented in figure 9 and figure 10 and are compared with experimental data obtained with respectively microthermocouples (diameter 20 μm), a laser-doppler anemometer and a detailed gaschromatographic analysis [15]. Experimental probability density functions for the temperature, compared with calculated values for the equilibrium and the partial equilibrium model were shown earlier in figure 3. For the temperatures the agreement between calculation and experiment is very good for both the equilibrium and the partial equilibrium: however the last model is to be preferred because of the better agreement in PDF values. The difference in temperature predicted by subsequently the elliptic and the parabolic computational scheme as shown in figure 9 for the equilibrium composition model is small and is also typical for calculations using the other combustion models. The main conclusion to be drawn from figure 9 is that the frequently applied frozen composition model leads to an unrealistic short flame length and too high a maximum temperature. Considering also figure 3 (and figure 16) the partial equilibrium model appears to be more realistic than the equilibrium model.
From figure 9 further a small shift in the position of the predicted flame front given by the maximum temperature is observed in comparison with the experimental data. This is possibly caused by inperfections in the turbulence model. However, optimalisation of the chosen turbulence constants is omitted.
The axial profiles for velocity and mixture fraction presented in figure 10 show the mutual deviations between the distinct numerical procedures and combustion models to be rather small for these quantities. The difference between measurements and predictions is much larger, however, particularly near the burner. The cause being that the flame was lifted to a height of x/D = 9 above the burner mouth. The agreement further down stream stems from the enhanced mixing by buoyancy forces, these causing high axial velocities around the maximum temperature region. Predictions with a somewhat more elaborate combustion model, designed a.o. to predict ignition, are depicted in figure 10 by the curves c. The agreement is very good for both the velocity and mass fraction; the temperature curves as presented in figure 9, do not change in the new model. More details on the improved combustion model will shortly be published, after completion of its development.

3.2.3. Radiation prediction.

Allthough the radiant heat transfer in the diffusion flame investigated is relatively small it provides an opportunity to test the various radiation models.
Experimental data obtained with the Shell radiation pyrometer [15] are given in figure 11 together with predictions using the equilibrium and partial equilibrium combustion models and various radiation models. For the simple one gray gas model (α_k = 0.4) gave a higher (radial) radiative heat transfer than the partial equilibrium model reflecting the fact that the maximum temperatures are higher for

the equilibrium model (see figure 3). The maximum value of the measured radiative heat flux lies between the two predicted values. The predictions based on the IFRF correlation ([11], 3 gray/1 clear gas, verified for natural gas only) show good agreement with the measurements. However, the computing time using this correlation was much higher, while the improvement of the prediction was smaller than the influence of the combustion model. Therefore the simple radiation model was preferred for subsequent furnace calculations.

3.2.4. Pollutants prediction.

The calculation of NO formation is devided in 'prompt NO' formation and 'thermal NO' formation in the manner discussed before. The 'prompt NO' values are given separately in figure 12 and appear to be fairly independent of the combustion model used. However, as shown in figure 2, lifting of the flame (equivalent to pre-mixing!) influences the NO concentration. So, using the improved combustion model (section 3.22), to estimate the lift of the flame, calculations of prompt NO concentrations have been made both for the lifted and the attached flame. The results show that in the attached flame the maximum prompt NO concentration is found well inside the fuel rich part of the flame; in both flames $Y_{f,st}$ is reached at x/D = 80. For the lifted flame, however, the maximum prompt NO concentration occurs near the stoichiometric point, as does the maximum NO concentration.
The thermal NO profiles calculated for the different combustion models are also shown in figure 12. They reflect the important influence of the temperature on the NO formation. The thermal NO formation in the frozen composition and the equilibrium model is substantial, because in these models the adiabatic combustion temperatures can be reached. However, the measured results from figure 3 indicate that the low thermal NO profiles obtained with the partial equilibrium model must be considered as being the most reliable. Addition of the preferred 'thermal NO' and 'prompt NO' profiles leads to a total NO profile comparing fairly well with the profile measured with the chemoluminescent method [15]. The shift to the richer part of the calculated profile compared with the measurements might be due to the fact that part of the 'prompt NO' is decomposed to HCN, not measured here. However, it is more likely that the flame is simply some 10 D shorter than the predicted one. A similar shift is also reflected in the temperature profile in figure 9 (curves a and b).
The identified importance of 'prompt NO' is largely in accordance with the results obtained by TAKAGI e.a. [28], in propane diffusion flames. In most other investigations the role of the 'prompt NO' is wrongly overlooked.

3.3. Cylindersymmetrical furnace calculations.

To test the models for furnace applications we used the extensive experimental data obtained in the Delft furnaces equipped with a newly designed central air burner (CAB) [29]. The CAB was designed to combine a stable combustion process, with easy dual fuel burning and low NO formation. The basic idea is that introduction of the gas through an annulus around a cylindrical airjet leads to a small effective hydraulic diameter of the gasflow and consequently to flames with a short reaction zone, a low residence time in the reaction zone and a low total NO formation. Calculations were made to test this hypothesis. Moreover several additional calculations have been made using central gas burners (CGB) in order to investigate the influence of scaling up of the furnace on NO formation.

3.3.1. CAB calculation and measurement.

The CAB calculations concerned a CAB, burning Groningen natural gas with a capacity of .75 MW, at an overall equivalence ratio of .98, and producing a flame essentially attached to the burners.
The main dimentions of the system are: primary air stream, diameter 95 mm, width of annular gas slot 6 mm, furnace diameter 0.6 m, length of (horizontal) furnace 5 m. The walls of the furnace are cooled to about 350 K by means of water.
Gravity effects have been neglected because no influence of buoyancy was detected in the experiments. The initial velocity profiles are not known, but aerodynamic resistances (wire mesh in the gas flow, perforated plate in the air flow) are applied to make them uniform. The furnace walls (estimated emmisivity = .8) are water cooled and have been assumed to be smooth; the short chimney at the end of the furnace is replaced by sudden enlargement, for reasons of simplicity.
Following GÜNTHER [32] we define the radiative heat transfer in the furnace with the dimensionless THRING number: $Th = \frac{\dot{m}\, h_c}{S\, \dot{q}_{rc}}$, where $\dot{m}$ is the mass flow, h_c the specific enthalpy for a stoichiometric natural gas-air mixture, (h_c = 2.8 MJ/kg), S is the furnace wall surface and $\dot{q}_{rc}$ the radiative heat flux calculated with the adiabatic flame temperature of natural gas with a emissivity a = .4 ($\dot{q}_{rc}$ = .53 MW/m^2). The THRING number is often referred to as the reduced firing density; in our case its value amounts to .3.
For the convective heat transfer and for similarity in the gas flow the CRAYA-CURTET number, defined before, and the burner Reynolds number have been applied as similarity parameters, following KANG e.a. [29]. The numerical values are Ct = .18 and $Re_b = 2.10^5$ (Re_b refers to the air flow).

The axial temperature and NO mass fraction profiles together with experimental data are presented in figure 13. The substantial difference between the predicted and measured temperature profiles thereby suggesting an unrealistic forward position of the flame. The two combustion models as such lead to limited differences in the predicted temperatures.
It has often be observed that the pyrometer tends to stabilize the flames, presumably due to the 2.5 cm diameter suction pyrometer used for the temperature measurements.
As for the calculated NO mass fraction profiles agreement results between the results of the partial equilibrium model and the measured Y_{NO} profile is striking, apart from the axial shift mentioned earlier. The calculated thermal NO contribution is very small (> 1 ppm for the partial equilibrium, and < 3 ppm for the equilibrium model; consequently nearly all NO predicted is due to 'prompt NO').
The differences in the temperature profiles are reflected in the predicted heat flux profiles at the furnace wall (see figure 14), most notably downstream of x/D_f = 3. However, for both combustion models the total local heat flux corresponds fairly well with the measured values (determined with an accuracy of ± 3% from the heat balance of the water, cooling the distinct wall segments).

The results of separate measurements of the radiative heat flux, using an ellipsoïdal pyrometer and the predicted radiation are depicted in the lower curves of figure 14. The discrepancy between measured and calculated radiative heat fluxes is not clear and is possibly due to an incorrect angle dependent sensitivity of the used pyrometer.
The large contribution of the convective heat transfer to the total heat transfer particularly near the maximum, should be noted.
The double peaked value of the total heat flux found with the partial equilibrium model is due to two peaks in the convective heat transfer curve. From these and other calculated data it appears that the dip in the heat transfer curve as $x/D_f = 3$ occurs at some distance beyond the end of the recirculation zone. This position corresponds well with the end of the recirculation zones that was calculated to be situated between $x/D_f = 2 - 3$ for isothermal flow and Ct = .212 - .675 (figure 5).
The first peak can be traced back near the point of reattachment to a high value of the turbulent kinetic energy. This higher turbulent level leads to heat transport to the wall. The second peak is due to the maximum in the temperature of the gas near the wall, occurring some distance beyond the reattachment point in this case.
Further support of the reliability of our predictions of the excessive heat transfer around the recirculation zone was obtained from experimental data of KRALL e.a. [30]. Calculations for a geometry similar to his experimental setup and at Ct number within the experimental range (.25 - .66) resulted in the same sharp increase in heat transfer in the recirculation zone as observed [31].
The quantitative agreement between Krall's measurements and our predictions was satisfactory, indicating that the calculation method is well founded.

3.3.2. Influence of furnace size on NO formation and flame length.

Because the prediction method of NO and the wall heat transfer has been shown to give realistic results for smaller furnaces, some scouting calculations were made to test its applicability for larger furnaces dimensions and furnace loads. The calculations were restricted to the vertical cylinder symmetrical open ended furnace.
The similarity parameters were kept constant at Ct = .18 and Th = .3; these values being chosen because of their frequent occurence in real furnaces.
As for the burners the primary gas flow diameters were taken at .03, .09 and .27 m, and the burner loads at 1.9, 17.1 and 155 MW. The overall equivalence ratio was taken equal to .96 and the gas velocity equal to 75 m/s in all three cases. The corresponding burner Re numbers are 2.10^5, 18.10^5 and 160.10^5. The velocity in the annular streams of air surrounding the cylindrical gas stream was set at 25 m/s.
The predicted mean 'thermal NO', 'prompt NO' and 'total NO', concentrations at the furnace outlet are given in figure 15. The furnace size is characterized by the parameter $D_h/\bar{u}_b$ (D_h = hydraulic diameter of gas flow, $\bar{u}_b$ = mean flow velocity at the burner); for the geometrially similar furnaces considered this parameter is proportional to the residence times of the gas in the flame zone and in the furnace as a whole. Relating the parameter to the chemical reaction rate yields the earlier defined Damköhler number.
From the results it can be concluded that for the burner and furnace dimensions investigated, most of the NO formed is 'prompt No'. However, $D_h/\bar{u}_b > 1.5\ 10^{-2}$, which corresponds to Da > 200, the 'thermal NO' formation becomes dominant.
The calculated flame length, being defined as the distance between the burner mouth and the point were the maximum temperature is reached and nearly all fuel has been burned, is shown in figure 16 and compared with several data obtained from the scarce literature.
The flame length for large vertical enclosed diffusion flames might become a more important parameter in the future due to the tendency to build more furnaces using bottom fired large diffusion flames. With an ensemble of these slender well defined times it is easier to exploit the available furnace volume optimally, than with strongly swirling flames [34].
It is clear from figure 16 that the calculations show the same trend as the measurements quoted by GÜNTHER [32] and NIEPENBURG [34]. Yet the predicted flame lengths are considerably larger; this may be due to the fact that weak swirl is often applied in the measured practical flames. The calculated data points can be matched with the correlation:

$L = .21(\dot{Q})^{0.5}$, where L stands for the flame lengths (in m) and $\dot{Q}$ is the burner load (in MW).

CONCLUSIONS

From the presented comparisons between measurements ans calculations, a number of pertinent conclusions can be drawn.

1. Out of the presented combustion models for natural gas diffusion flames, the so-called partial equilibrium composition model gives the best general agreement between theoretical and experimental results.
2. The equilibrium composition model might be satisfying for the prediction of the mean flow and temperature field, but it predicts too large temperature fluctuations and too high instantaneous temperatures; consequently it is less suitable for estimating the temperature dependent NO formation.
3. The frequently used frozen composition model clearly leads to erroneous results.
4. It can be expected that the partial equilibrium conditions depend on the turbulent stretch in the flow, but measurements in natural gas flames with different stretch levels [15], characterized by Da = 2-200, reveal that in practical diffusion flames the influence of stretch is very small. Because of the high hydrocarbon content of Groningen natural gas, it can be anticipated that these conclusions are generally valid for hydrocarbon flames.
5. Further it is found that the thermal NO formation in non-preheated hydrocarbon flames is relatively small, particularly for the small and medium size hydrocarbon flames used in experimental studies. On the contrary the contribution of prompt NO is particularly relevant; its formation is satisfactory modelled in our study.

6. When interpreting NO data in diffusion flames one has to be carefull when dealing with lifted flames. In that case the NO mass fraction profiles in the fuel rich region derived from prompt NO formation can be changed completely, due to premixing with air.
7. Taking into account mixture fraction fluctuations, calculations using the k-ε-turbulence model have been made for isothermal furnace flows; the results were found to be in general agreement with experimental data [5, 6]. Subsequent furnace calculations show a very good agreement between measurements and calculations for the NO mass fraction and the total wall heat transfer.
8. Further the calculations lead to the conclusion that in the slender cylindrical furnaces investigated, characterised by Th = .3, Ct = .18 and $Re_b = 210^5$, the contribution of convective heat transfer dominates in the total wall heat flux particularly in the recirculation zone.
9. The parameter study finally shows that the applied numerical technique is well suited for the prediction of the influence of furnace size and proportions on such quantities as NO formation, flame length and heat transfer. However, further validation of the method is required in this field.

ACKNOWLEDGEMENTS

The authors like to acknowledge the cooperative support provided by prof. D.B. Spalding and dr. A.S.C. Ma of Imperial College, London in arranging the basic computer program used in the present calculations and developed by Combustion, Heat and Mass Transfer Ltd.

REFERENCES

1 OSGERBY, I.T.,
Literature Review of Turbine Combustor modeling and emissions.
AIAA journal, 6 (1974), p. 743.

2 KHALIL, E.E., SPALDING, D.B. and WHITELAW, J.H.
The calculation of local flow properties in two-dimensional furnaces.
Int. J. Heat Mass Transfer, 18 (1975), p. 775.

3 HUTCHINSON, D, KHALIL, E.E. and WHITELAW, J.H.
The calculation of wall heat transferrate and pollutant formation in symmetric furnaces.
4th Members conf. IFRF, paper I3, Noordwijkerhout, (1976).

4 MICHELFELDER, S., BARTELDS, H. LOWES, T.M. and PAI, B.R.
Berechnung der Wärmeflusses und der Temperaturverteilung in Verbrennungskammern.
VDI Berichte 211 (1974), p. 23.

5 BECKER, H.A., HOTTEL, H.C. and WILLIAMS, G.C.
Mixing and flow in ducted turbulent jets.
9th Int. Symp. on Combustion (1963), p. 7.

6 BECKER, H.A., HOTTEL, H.C. and WILLIAMS, G.C.
Concentration fluctuations in ducted turbulent jets.
11th Int. Symp. on Combustion (1967), p. 791.

7 LAUNDER, B.E. and SPALDING, D.B.
Mathematical models of turbulence.
Academic Press (1972) London.

8 GOSMAN, A.D. and LOCKWOOD, F.C.
Incorporation of a flux model for radiation into a finite-difference procedure for furnace calculations.
14th Int. Symp. on Combustion (1972), p. 661.

9 LAUNDER, B.E., MORSE, A. RODI, W. and SPALDING, D.B.
The prediction of free shear flows - a comparison of six turbulence models.
NASA Conf. on Free Shear Flows, Langley (1972).

10 KANG, Y.M. and SUZUKI, K.
Numerical study of confined jets, a prediction of flow pattern and turbulence quantities.
Mem. of the faculty of Engng, Kyoto University, Vol. XL (1978), p. 41.

11 LOWES, T.M., BARTELDS, H. HEAP, M.P., MICHELFELDER, S. and PAI, B.R.
The prediction of radiant heat transfer in axi-symmitrical systems.
IFRF report G02/a/25 (1973), IJmuiden.

12 EDWARDS, D.K. and BALAKRISHAN, A.
Thermal radiation by combustion gases.
Int. J. Heat Mass Transfer, 16 (1973), p. 25.

13 BRAY, K.N.C. and MOSS, J.B.
A unified statistical model of the premixed turbulent flame.
Acta Astronautica 4 (1977), p. 291.

14 VAN DUYVENVOORDEN, C.
Benadering van fysische en chemische grootheden uit rookgassen van Groningen aardgas/lucht mengsels door Chebyshev dubbel polynomen (in Dutch).
Laboratorium voor Energievoorziening, Rep. VS7703 (1977), Delft.

15 PAAUW, Th. T.A.
Nitrogenoxide formation in turbulent natural gas flames.
Dissertation, Technical University Delft (to be published in early 1980).

16 BECKER, H.A.
Concentration fluctuations in ducted jet mixing.
Ph. D. Thesis (1961), Mass. Inst. Techn.

17 HABERDA, F.
Die berechnung turbulenter diffusionsflammen unter berücksichtigung von Konzentrationsschwankungen.
Ph. D. Thesis (1977), Karlruhe.

18 BULAU, J.R.
Radical overshoots and dissociation in methane/air flames.
Journal of Chem. Phys. 62 (1975) 3605.

19 EBERIUS, K.H. and JUST, Th.
NO formation in fuel rich flames, a study of the influence of the hydrocarbon structure.
Agard Conf. Proc. no. 125 (1973), pp. 16-1.

20 LOCKWOOD, F.C. and NAGUIB, A.S.
The prediction of the fluctuations in the properties of free round jet turbulent diffusion flames.
Comb. and Flame 24 (1975), p. 109.

21 WILLIAMS, F.A.
Combustion Theory.
Addison Wesly Publ. (1965), Reading Mass.

22 PUN, W.M. and SPALDING, D.B.
A general computer program for two-dimensional elliptic flows.
Imperial College, M.E. Dept. Rept. HTS/76/2, (1976).

23 PATANKAR, S.V. and SPALDING, D.B.
Heat and Mass transfer in boundary layers.
Intertext Books (1970), London.

24 SPALDING, D.B.
Concentration fluctuations in a round turbulent free jet.
Chem. Engng. Sc. 26 (1971), p. 95.

25 TAKAGI, T, OGASAWARA, M, FUJII, K. and DAIZO, M.
A study on nitric oxide formation in turbulent diffusion flames.
15th Int. Symp. on Combustion (1975), p. 1051.

26 VAN WEES, F.G.H.
Metingen aan de centrale luchtbrander.
Laboratorium voor Energievoorziening, Rep. VS7403, (1974), Delft.

27 VAN STAA, H.
Private communication.

28 THRING, M.W.
Application of Similarity principles to thermal transport systems.
Nature 159 (1947), p. 203.

29 KANG, Y, SUZUKI, K. and SATO, T.
Convective heat transfer in an axi-symmetrical confined jet.
(1979) to be published.

30 KRALL, K.M. and SPARROW, E.M.
Turbulent heat transfer in the separated reattached and redevelopment regions of a circular tube.
J. Heat Transfer 88 (1966), p. 131.

31 SUZUKI, K.
A numerical study on fluid mechanics and heat transfer in recirculating flows.
Laboratorium voor Energievoorziening, Rep. EV1011 (1977), Delft.

32 GÜNTHER, R.
Verbrennung und Feuerungen.
Springer Verlag (1974), Berlin, pp. 284, 414.

33 QUAN, V, KLIEGEL, J.R., DE VOLO, N.B. and TEXEIRA, D.P.
Analytic scaling of flow field and nitric oxide in combustors.
Comb. Sc. and Techn. 9 (1974), p. 209.

34 NIEPENBERG, H.P.
Entwicklungstendenzen im grossbrennerbau, in Industrieöfen und-Feuerungen.
Ed. K. Giesen, Haus der Technik (1972), p. 28.

NOMENCLATURE

$C_{\varepsilon_{1,2}}$, $C_{f_{1,2}}$, C_D	constants in turbulence model
D	diameter
E	wall function parameter
E_z	action energy
f	variable
g	gravitation constant
h	stagnation enthalpy
h_c	mixture averaged heat of reaction
K	wall function constant
k_z	pre-exponental factor
k	turbulent kinetic energy
L	flame length
M	molecular weight
$\dot{m}$	mass flow
p	pressure
$\dot{Q}$	thermal load
$\dot{q}_r$	radiation wall heat flux
R_r^k, R_x^k	radiation heat flux in r and x direction
r	radial distance
r	stoïchiometric fuel-oxygen mass ratio
S	furnace wall area
T	temperature
T_i	chebyshev polynomial of order i
u	velocity
V_o^*	characteristic velocity in Ct
$\bar{v}_f$, $\bar{v}_o$	averaged velocity over furnace, burner area
$\bar{v}_F^2$	averaged square velocity over furnace area
v	radial velocity
$\dot{w}$	reaction rate
x	axial distance
X	mole fraction
Y	mass fraction
Y_f	mixture fraction
Y_f'	square of mixture fraction functions
α_k	absorption coefficient
ε_k	emmission coefficient
ε	turbulent kinetic energy dissipation
ϕ	equivalence ratio
μ	viscosity
ρ	density
σ	Stefan-Boltzmann constant
τ_c	characteristic reaction time

SUBSCRIPTS

b	burner
e	effective
f	furnace or duct
fu	fuel
ox	oxidant
i	chemical species
k	gray gas
o	inlet condition
st	stoïchiometric
w	wall

DIMENSIONLESS NUMBERS

Ct	Craya-Curtet number
Da	Damköhler number
Fr	Froude number
Re	Reynolds number
Th	Thring number
σ	Prandtl number

TABLE I PHYSICAL QUANTITIES TO BE SUBSTITUTED IN CONSERVATION EQUATION (1)

Quantity	ϕ	ρ_ϕ	μ_ϕ	S_ϕ
Mass	1	ρ	o	o
Axial momentum	u	ρ	μ_e	$\frac{\partial}{\partial x}(\mu_e \frac{\partial u}{\partial x}) + \frac{1}{r}\frac{\partial}{\partial r}(\mu_e r \frac{\partial v}{\partial x}) - \frac{\partial p}{\partial x} + \rho g_x$
Radial momentum	v	ρ	μ_e	$\frac{\partial}{\partial x}(\mu_e \frac{\partial u}{\partial r}) + \frac{1}{r}\frac{\partial}{\partial r}(\mu_e r \frac{\partial v}{\partial r}) - 2\mu_e \frac{v}{r^2} - \frac{\partial p}{\partial r}$
Turbulent kinetic energy	k	ρ	$\frac{\mu_e}{\sigma_k}$	$G_{k1} - \rho\varepsilon$
Dissipation rate	ε	ρ	$\frac{\mu_e}{\sigma_\varepsilon}$	$\frac{\varepsilon}{k}(C_{\varepsilon 1} G_{k1} - C_{\varepsilon 2}\rho\varepsilon)$
Stagnation enthalpy	h	ρ	$\frac{\mu_e}{\sigma_h}$	$\Sigma_k (2\overline{\alpha_k}(R_x^k + R_y^k) - 4\sigma\overline{\varepsilon_k T^4}$
Mixture fraction	Y_f	ρ	$\frac{\mu_e}{\sigma_f}$	o
Mixture fraction fluctuations	Y_f'	ρ	$\frac{\mu_e}{\sigma_f}$	$C_{f1} G_{f1} - C_{f2}\rho\frac{\varepsilon}{k} Y_f'$
NO mass fraction	Y_{NO}	ρ	$\frac{\mu_e}{\sigma_f}$	$\overline{\rho\dot{w}}_{NO}$
Radial radiant total heat flux gas k	R_r^k	o	$\frac{1}{\bar{\alpha}_k + 1/r}$	$-\bar{\alpha}_k R_r^k + \sigma\overline{\varepsilon_k T^4}$
Axial radiant sun heat flux gas k	R_x^k	o	$\frac{1}{\bar{\alpha}_k}$	$-\bar{\alpha}_k R_x^k + \sigma\overline{\varepsilon_k T^4}$

$$G_{k1} = \mu_e \left(2\left(\left(\frac{\partial u}{\partial x}\right)^2 + \left(\frac{\partial v}{\partial r}\right)^2 + \left(\frac{v}{r}\right)^2\right) + \left(\frac{\partial u}{\partial r} + \frac{\partial v}{\partial x}\right)^2\right)$$

$$G_{f1} = \mu_e \left(\left(\frac{\partial Y_f}{\partial x}\right)^2 + \left(\frac{\partial Y_f}{\partial r}\right)^2\right)$$

TABLE II COMPILATION OF MODEL CONSTANTS

Fuel constants:

Slochteren natural gas (vol. %) CH_4 - 81.3, N_2 - 14.4, C_2H_6 - 2.9 + higher hydr.

r = 13.07

Turbulence constants:

$C_{\varepsilon 1}$ = 1.40, $C_{\varepsilon 2}$ = 1.92, C_D = .09, C_{f1} = 2.8, C_{f2} = 2.0, K = .40, E = 9.0

Prandtl numbers:

σ_k = 1.0, σ_ε = 1.3, σ_ϕ = .7

TABLE III

Grid location in the case of grid I and II from figure 8.

Radial grid locations grid I:

r/D = 0.0, 0.25, .50, .75, 1., 1.5, 2.5, 4.0, 5.5, 7.0, 9.0, 11., 13., 17., 21., 25., 29., 33., 37., 41., 44., 47., 49., 50.

Radial grid locations grid II:

r/D = 0.0, .125, .25, .50, .75, 1.0, 1.25, 1.8, 2.2, 2.7, 3.3, 4.0, 4.8, 5.5, 7.0, 8.4, 10.1, 12.0, 14.4, 17.2, 20.6, 24.7, 29.7, 35.6, 40.6, 45.6, 48.5, 49.5, 50.

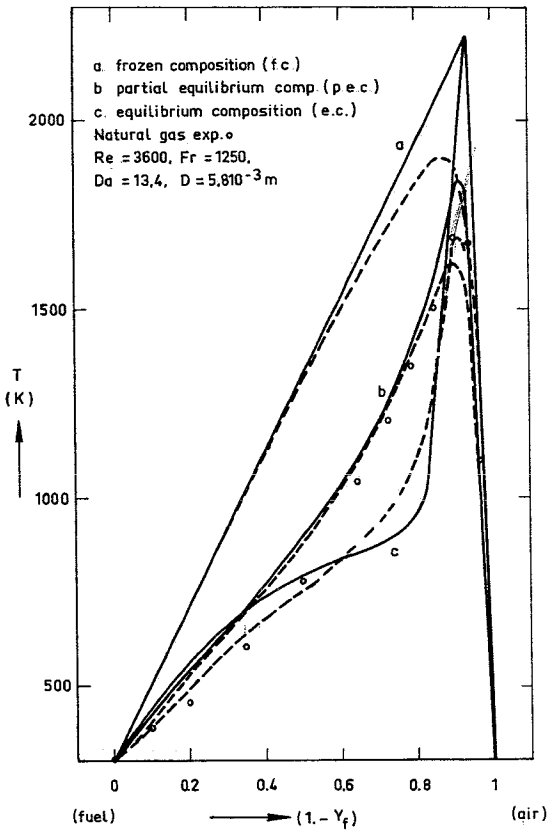

fig. 1a. Theoretical temperature as a function of the mixture fraction for different combustion models and experimental data obtained in a attached diffusion flame (dashed lines give the estimated influence of unmixedness).

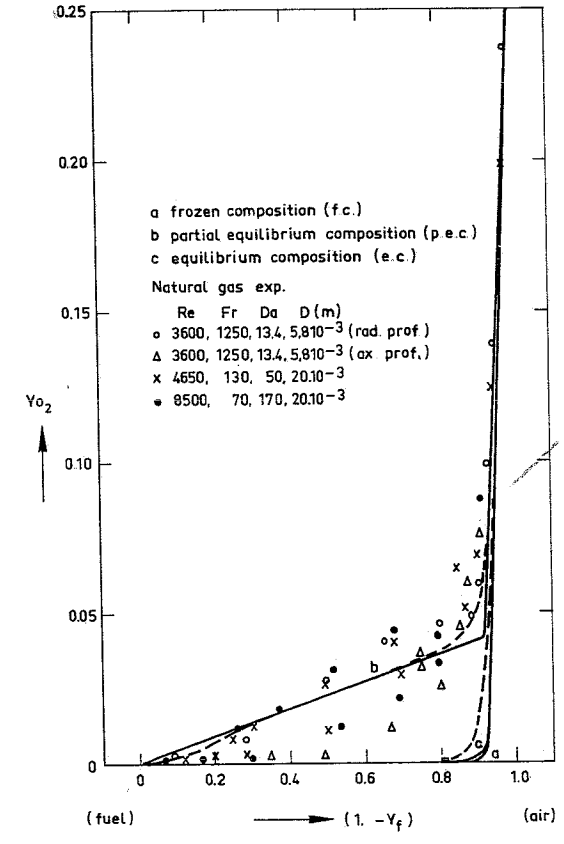

fig. 1b. Theoretical oxygen mass fraction as a function of the mixture fraction for different combustion models and experimental data obtained in attached diffusion flames (dashed lines give the estimated influence of unmixedness).

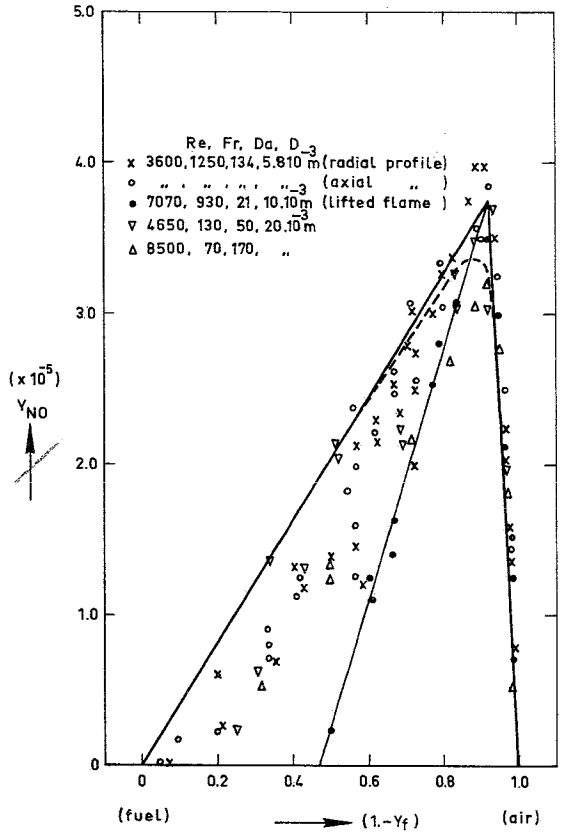

fig. 2. Theoretical prompt NO mass fraction as a function of the mixture fraction for a frozen composition prompt NO chemistry (maximum prompt NO level = 38 ppm) compared with experimental data obtained in diffusion flames. Dashed curve gives the estimated influence of unmixedness.

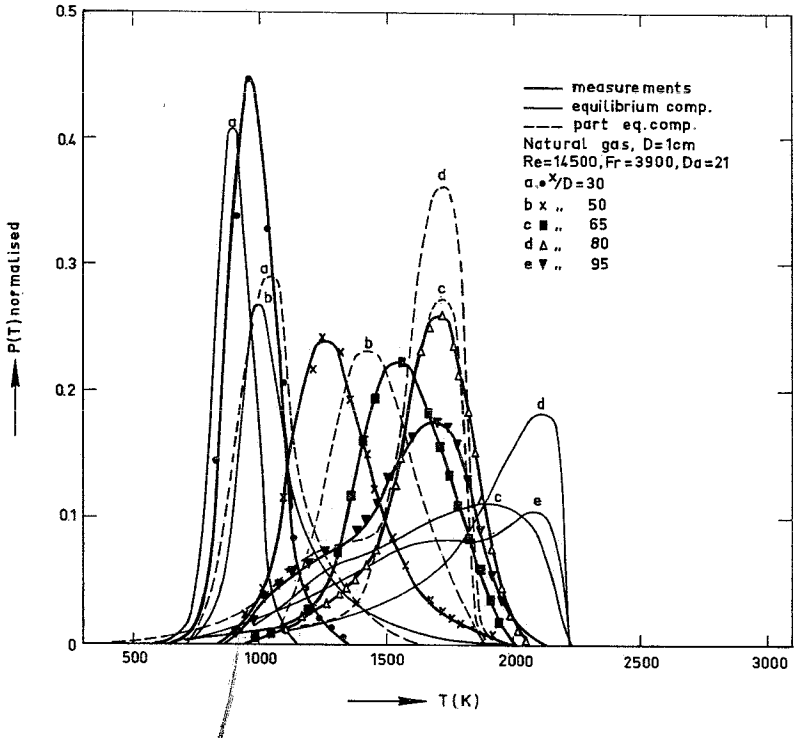

fig. 3. Measured normalised probability density functions for the temperature on the axis of a diffusion flame, compared with calculated P.D.F.'s obtained with different combustion models.

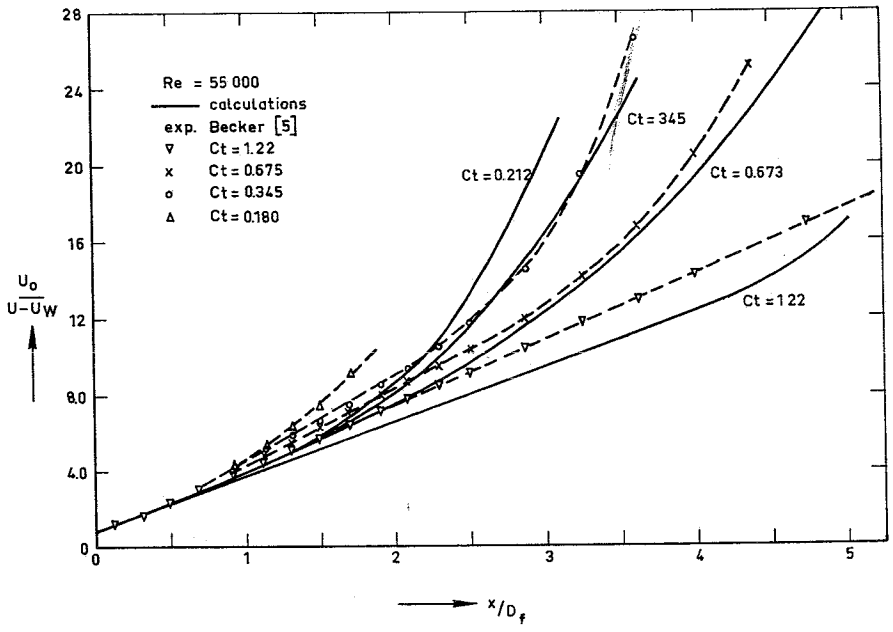

fig. 4. Calculated axial velocity decay in ducted isothermal jet flow compared with measurements.

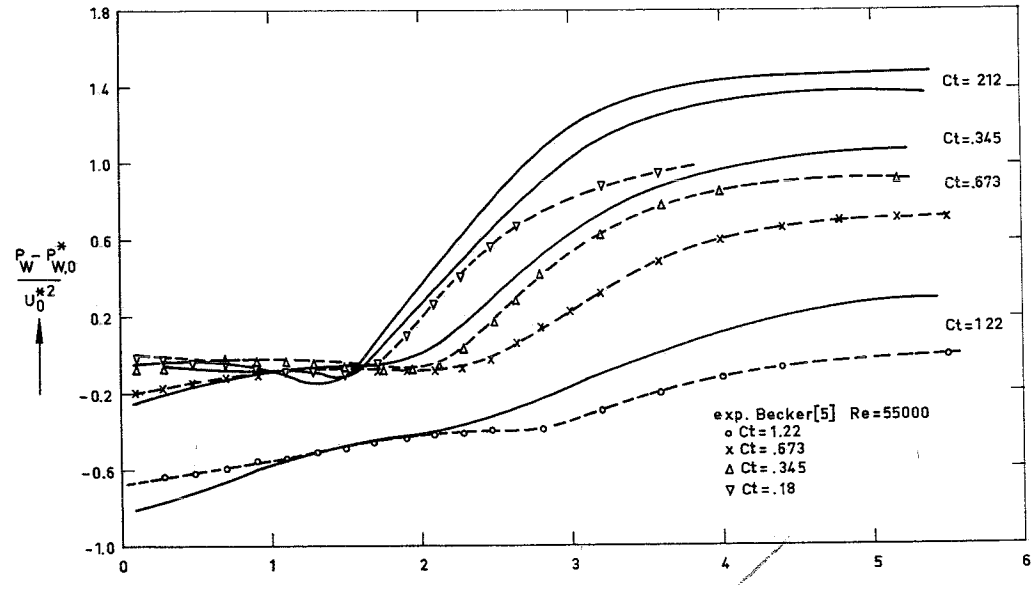

fig. 5. Calculated axial static pressure profiles at the duct wall compared with experiments for isothermal ducted jet flow ($P^*_{w,o} = P_{w,o} + v^{*2}_o/2.$).

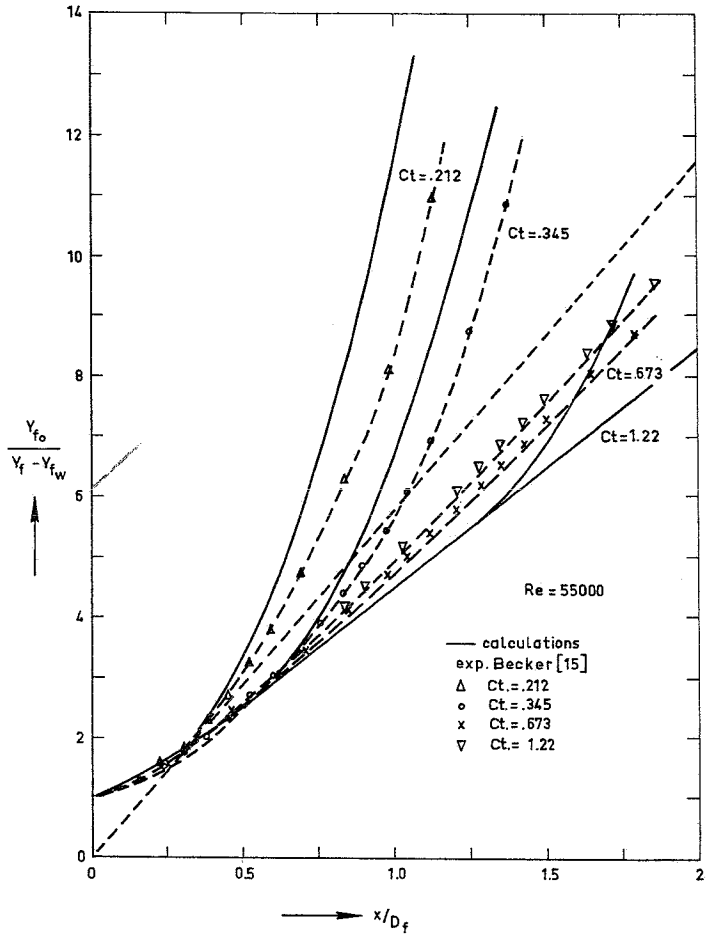

fig. 6. Calculated axial decay of the mixture fraction in ducted isothermal jets compared with measurements.

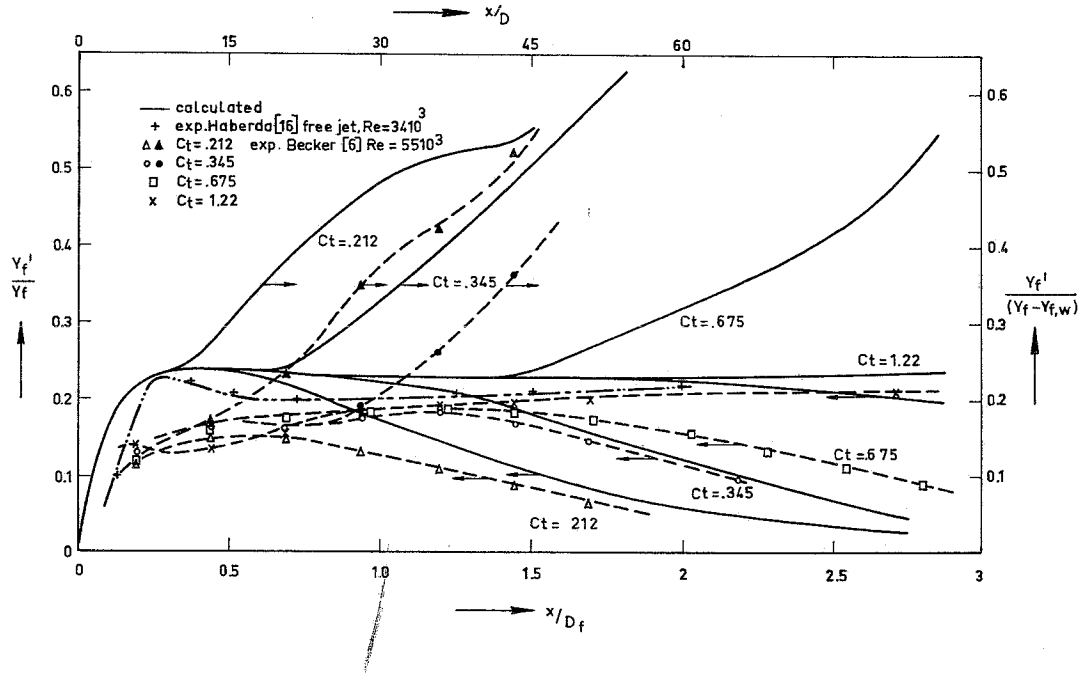

fig. 7. Calculated axial decay of the mixture fraction fluctuations in ducted isothermal jets (x/D_f) and in free jets (x/D), compared with measurements.

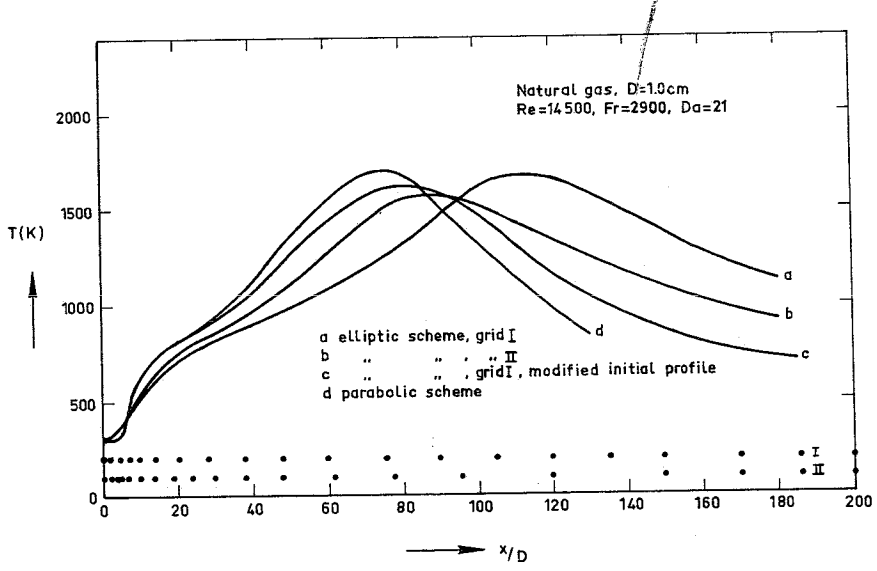

fig. 8. Calculated axial temperature profiles for a free turbulent diffusion flame using both a parabolic flow and an elliptic flow finite difference scheme. Also the influence of modifications in initial profile and grid arrangement are given (axial grid locations represented by dots and radial grid locations as given in table III).

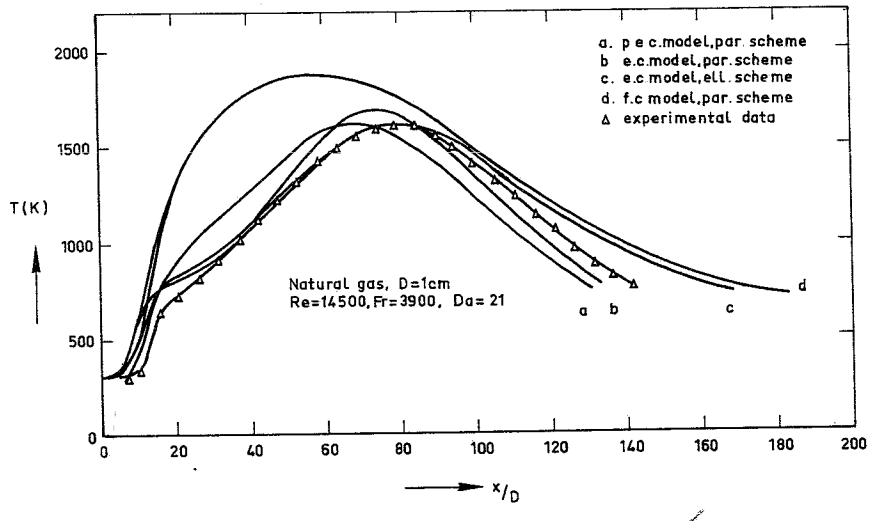

fig. 9. Calculated axial temperature profiles for a free jet diffusion flame using a frozen composition, equilibrium or partial equilibrium composition combustion model, compared with measurements.

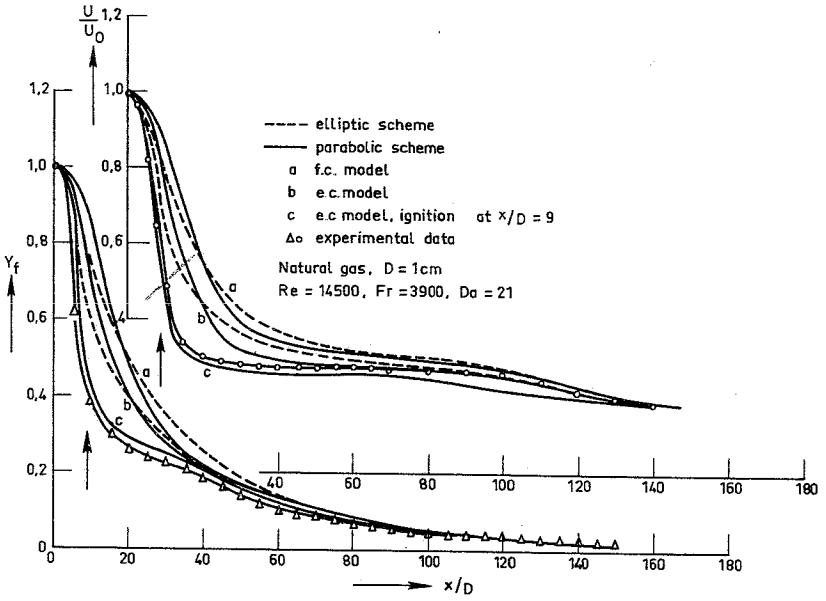

fig. 10. Calculated axial velocity and mixture fraction profiles for a free jet diffusion flame. (The arrow indicates the calculated and measured ignition point).

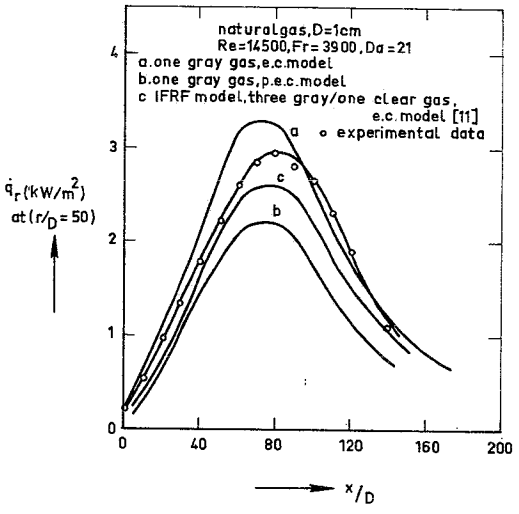

fig. 11. Calculated radial radiation fluxes at r/D = 50, for turbulent diffusion flames and various combustion and radiation models, compared with experimental data.

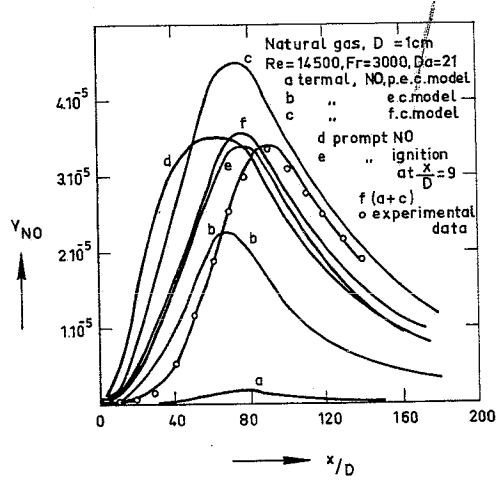

fig. 12. Calculated and measured axial nitrogenoxide profiles of the turbulent diffusion flame in case of thermal and prompt NO formation.

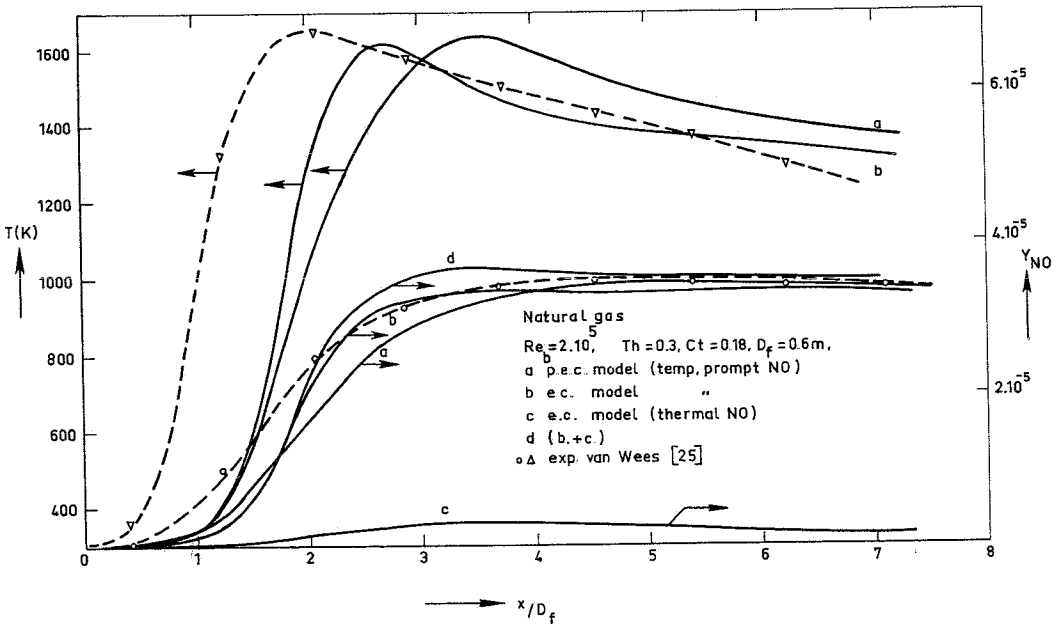

fig. 13. Measured and calculated axial nitrogenoxide and temperature profiles in an axisymmetrical natural gas fired furnace, equipped with a central-air burner.

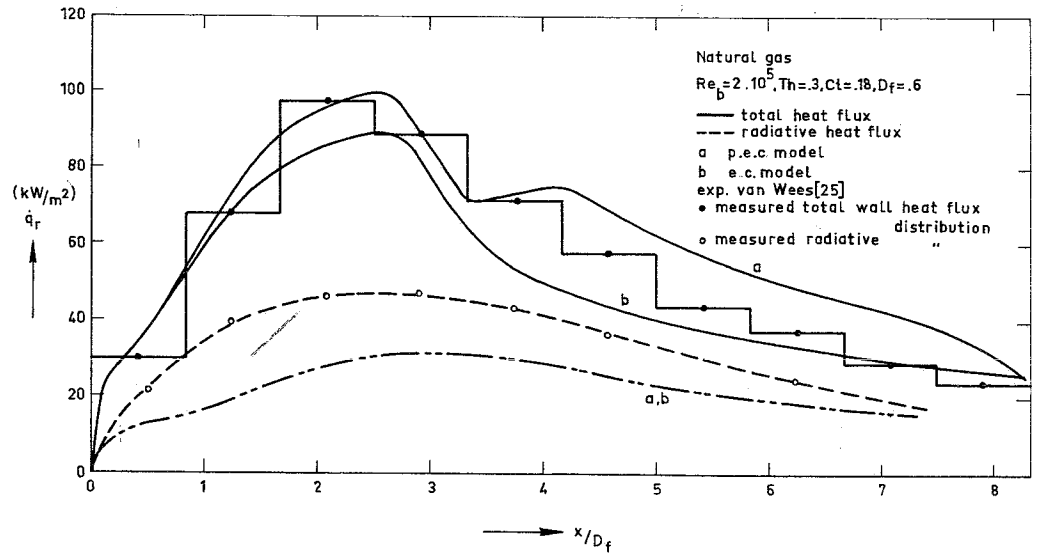

fig. 14. Measured and calculated radiative and total wall heat flux distribution at the furnace wall of an axisymmetrical natural gas fired furnace (central-air burner).

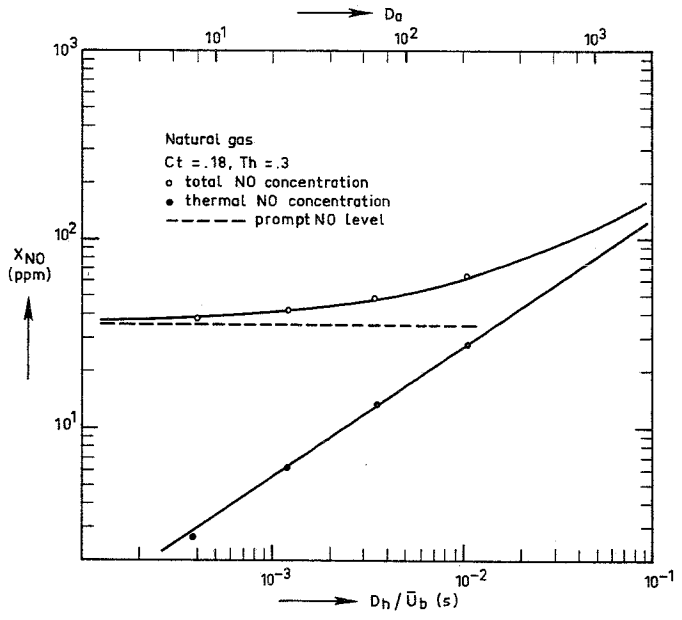

fig. 15. Calculated influence of (cylindrical) furnace size on prompt NO, thermal NO and total NO concentration. Furnace dimensions proportional to burner diameter. Furnace size characterised by time parameter $D_h/\bar{u}_b$ (D_h = hydraulic diameter of entering gas flow). The point with lowest thermal NO concentration represents the central-air burner calculation.

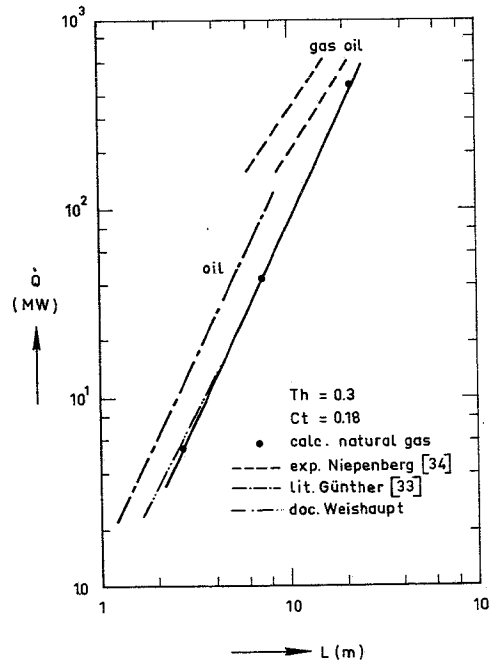

fig. 16. Correlation between burner load and flame lenght for vertical, cylindrical, natural gas fired furnaces, and some experimental data.

DISCUSSION

H.Eickhoff, Ge

Did you measure and predict CO-concentrations also? If so, how well do they agree and especially what is your highest predicted CO-concentration?

Author's Reply

The maximum CO mass-fraction predicted with the partial equilibrium composition model is about 3%, a value that compares well with the measured maximum CO mass-fractions. CO mass-fractions calculated with the frozen composition model are very low, while CO mass-fractions calculated with the equilibrium model can reach much too high values, up to 10%.

N.Peters, Ge

Let me first congratulate you for this well documented piece of work. Also I would like to comment on the relatively large oxygen values that you find on the fuel rich side of the flame. I would think that this is rather due to turbulence effects than to quenching. In a comment to Janicka's and Kollmann's paper it was noted that the fuel rich shift of NO-production could be attributed to turbulence. I believe that a similar reasoning could be applied to the oxygen shift.

Author's Reply

In the first instance we have also tried to explain the too high oxygen mass-fractions on the fuel rich side with turbulence smearing out, or better unmixedness. When we take into account turbulent intensities of the mixture fraction at the fuel rich side, reaching a value of about 45% as calculated with the finite difference technique, we also obtain much too low values of the oxygen mass-fraction, as depicted in Figure 1b by the dashed line above c. Also we found high CO and H_2 mass-fractions up to respectively 3% and .3% mainly in the fuel rich side, which indicates that there, incomplete reaction has to take place. The chosen partial equilibrium model predicts well also these mass-fractions.

M.Nina, Po

Could you give some details on how the calculation scheme accommodates for the height of the lifted flame base.

Author's Reply

As noted in the paper the height of the lifted flame base chosen in Figure 10 is deduced from experiments. However a procedure has been worked out and presented before[1] to calculate this height in the calculation scheme. With this procedure we were able to reproduce the measured values accurately.

1. Paauw, Th.T.A. Bakker, R. *Use of the Well Stirred Reactor Concept for the Prediction of Flame Stablization*, 4th Members Conference, IFRF, Paper 15, Noordwykerhout (1976).